ACS OMEGA

http://pubs.acs.org/journal/acsodf

Article

Enhanced Conductivity via Extraction of Hydrocarbon Templates from Nanophase-Separated PEO–LiOTf Polymer Electrolyte Films

John W. Ostrander, Lei Wang, Teljan Ali Kizi, Jana A. Dajani, Austin V. Carr, Dale Teeters,* and Angus A. Lamar*

Cite This: *ACS Omega* 2020, 5, 20567–20574

Read Online

ACCESS | Metrics & More | Article Recommendations | Supporting Information

ABSTRACT: A series of poly(ethylene oxide)–LiOTf electrolyte films were prepared using a variety of hydrocarbon templates as nanofillers, resulting in observable nanophase separation in the polymer electrolyte. Upon partial extraction of the nanofiller template, an enhanced conductivity over 2 orders of magnitude was measured using ac impedance. Scanning electron microscopy, differential scanning calorimetry, and thermogravimetric analysis were employed to characterize the porosity, composition, and mass loss of template-extracted and nonextracted film samples.

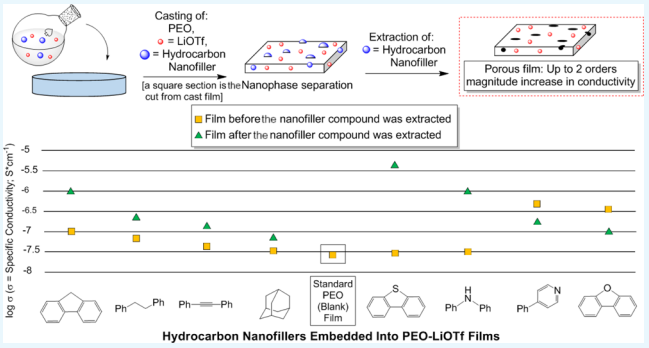

INTRODUCTION

The rapid development of technologies (i.e., smart phones, notebook computers, electric vehicles, and so forth) that utilize portable electrochemical energy storage devices has been accompanied by an intensified interest in the improvement to the batteries which power them. Lithium-ion batteries have been an energy storage device in great demand because of their high energy conversion efficiencies and low self-discharge values.[1−3] There has been an increasing shift toward solid polymer electrolyte (SPE) materials, such as poly(ethylene oxide) (PEO), because of enhanced flexibility, safety, and avoidance of a separator when compared to the corresponding liquid electrolytes.[4−7] The current disadvantage to SPEs, however, lies within the significantly lower ion conductivities when compared to the liquid counterparts.[1,8,9] To overcome this challenge, strategies to create a higher ionic conductivity have been attempted, which include the addition/use of (1) anodic doping agents;[10,11] (2) plasticizers;[12,13] (3) ceramic and clay fillers;[14−19] (4) block copolymers,[11,20−24] interpenetrating networks,[25,26] composites,[27,28] and nanopore filling[29] with polymer electrolytes; and (5) various nanoframeworks.[30−33] When considering the many areas of work done on increasing the ionic conductivity, much of the work can be categorized as creating nanoporosity in which to confine the polymer electrolyte.

Many of the methods to create highly nanoporous SPE films have disadvantages that can include laborious multistep procedures, low degrees of control regarding surface versus bulk porosity, high thermal treatment temperatures, and low yields.[34−37] Direct templating, an approach more akin to that found in molecular imprinting technology,[38] has been investigated in the quest to produce a more nanostructured SPE film with pores and potentially active interfaces. To date, templates employed in such an approach have consisted of silicates, metals/metal oxides, and separate polymeric units.[37] Removal of these templates requires a base (NaOH), an acid (HF, HCl, or H_3PO_4), or a carcinogenic solvent such as methylene chloride.[37] We envisioned the use of simple feedstock hydrocarbons as templates that would be selectively removed by rinsing a templated film with an innocuous nonpolar solvent. Herein, we describe the first example of a novel and highly practical means to generate PEO–$LiSO_3CF_3$ (PEO–LiOTf) films with enhanced conductivity via the selective extraction of nanophase-separated[10,37] SPE materials. In this approach, selective extraction of the hydrocarbon nanofiller creates surface pores and bulk cavities that allow for enhanced transport of the residual ions in the PEO–LiOTf film (Scheme 1). It is expected that this economical, operationally simple approach will lead to a new generation of porous polymer electrolytes with high ion conductivities.

RESULTS AND DISCUSSION

One key physical characteristic of a PEO–LiOTf electrolyte film involves its highly hygroscopic nature and significant

Received: June 12, 2020
Accepted: July 27, 2020
Published: August 7, 2020

Scheme 1. Our General Approach for Direct Templating with Hydrocarbon Nanofillers

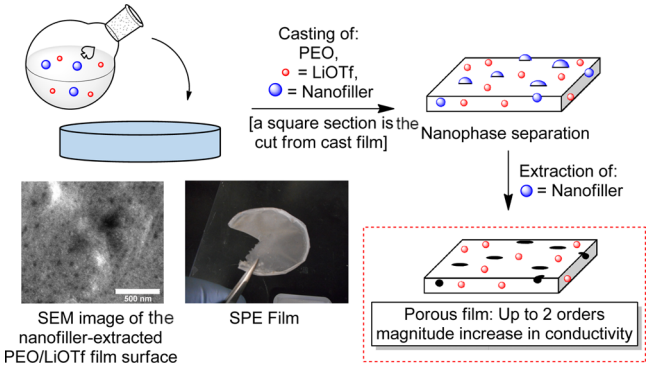

solubility in polar solvents. In stark contrast, these films will not dissolve or react in nonpolar hydrocarbon solvents such as hexanes. In the design of our investigation, we aimed to exploit this feature by selecting nanofiller materials (shown in Figure 1) that will dissolve in both acetonitrile (the solvent used to

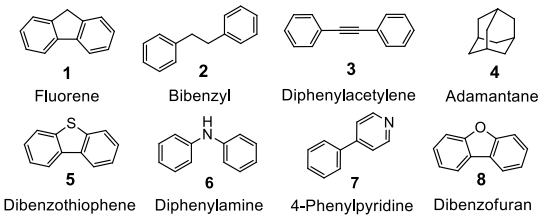

Figure 1. Hydrocarbon nanofiller molecules employed in the templating approach.

cast the films) and hexanes. A variety of relatively low-molecular-weight compounds with the representative structural features were chosen, including nonaromatic aliphatics, nonpolar and polar aromatics, conjugated and nonconjugated hydrocarbons, heterocycles capable of weak Li^+ coordination, and polar amines capable of strong Li^+ coordination.

Films were prepared using a casting method in which PEO and LiOTf (~15:1 PEO/LiOTf) along with a nanofiller compound were homogeneously dissolved in acetonitrile. After evaporating acetonitrile under a flow of nitrogen for 48 h, films were produced that were consistently between 90 and 110 μm thickness (see Figure S3A–C of the Supporting Information). The films were then soaked in hexanes and rinsed twice to extract nanofiller materials. The identity of the removed nanofiller was confirmed by ^{1}H NMR, and the quantity of the extract was determined by weighing the dried residual material and further verified via thermal gravimetric analysis (TGA) (see Figure S20A–F in the Supporting Information for the representative examples). The leaching of LiOTf or PEO into the hexane was not observed using ^{1}H and ^{19}F NMR in any of the examples.

To begin our investigation, adamantane was selected as a nanofiller, and a series of films were prepared using a range of loadings (5, 10, 20, and 40 mol % relative to LiOTf). Upon extraction of the nanofiller, very little difference was observed regarding the conductivity in comparison to the analogous nonextracted version. For all subsequent studies, a nanofiller loading of 20 mol % relative to LiOTf was selected as an optimal amount.

A series of hydrocarbons and heteroarenes (Figure 1, **1**–**8**) were chosen for investigation. The degree of extraction of the nanofillers ranged from 9 to 91% (Table 1) and may be

Table 1. Data Obtained from Hydrocarbon Nanofiller Nonextracted (1a–8a) and Extracted (1b–8b) PEO–LiOTf Films

entry	compound (nanofiller)	percentage of the compound extracted	name of the film	σ^a
1	none		PEO	2.681×10^{-8}
2	**1** (fluorene)	0	**1a**	1.392×10^{-7}
3	**1** (fluorene)	85	**1b**	8.848×10^{-7}
4	**2** (bibenzyl)	0	**2a**	6.507×10^{-8}
5	**2** (bibenzyl)	57	**2b**	2.581×10^{-7}
6	**3** (diphenylacetylene)	0	**3a**	4.206×10^{-8}
7	**3** (diphenylacetylene)	59	**3b**	1.429×10^{-7}
8	**4** (adamantane)	0	**4a**	3.640×10^{-8}
9	**4** (adamantane)	9	**4b**	5.791×10^{-8}
10	**5** (dibenzothiophene)	0	**5a**	2.905×10^{-8}
11	**5** (dibenzothiophene)	57	**5b**	4.707×10^{-6}
12	**6** (diphenylamine)	0	**6a**	3.096×10^{-8}
13	**6** (diphenylamine)	91	**6b**	1.109×10^{-6}
14	**7** (4-phenylpyridine)	0	**7a**	4.989×10^{-7}
15	**7** (4-phenylpyridine)	41	**7b**	2.425×10^{-7}
16	**8** (dibenzofuran)	0	**8a**	3.793×10^{-7}
17	**8** (dibenzofuran)	18	**8b**	8.618×10^{-8}

^{a}Specific conductivity (S* cm^{-1}).

influenced by the following factors: the degree of aggregation of the compounds, which may be a result of the solubility of the compounds in acetonitrile, and the solubility of the nanofiller compound in PEO, which may affect the inclusion of the nanofiller material into the bulk of the PEO film versus the surface.

The conductivity of the extracted and nonextracted PEO–LiOTf bulk films was measured at room temperature (20 °C) using ac impedance spectroscopy. In a control experiment, it was determined that subjecting a standard PEO–LiOTf film (without the nanofiller material) to the hexane extraction procedure had no effect on the conductivity. Each of the films with nanofiller materials was prepared in duplicate, and the ac impedance of the nonextracted (**1a**–**8a**) and extracted (**1b**–**8b**) films was measured separately. The Nyquist plots (imaginary vs real impedance) of films containing nanofillers **1**–**4** (Table 1, entries 1–9) are shown in Figure 2. The apparent resistance of each sample can be estimated by the intersection of the extrapolated semicircle of the data with the real impedance axis. Conductivity is inversely related to the diameter of the semicircle (i.e., conductivity increases as the x-intercept decreases in value). These data are then converted to specific conductance by taking into account the polymer configuration and the geometry of the cell (the contact electrode surface area and film thickness).[33]

As observed in Figure 2, the conductivity of both the nonextracted and extracted films slightly increases relative to the standard PEO. This may result from the colligative effect of the nanofiller additive disrupting the packing of the PEO matrix during the casting process, inherently creating a more porous film. This factor will be discussed later. Upon extraction of the nonpolar hydrocarbon nanofillers with hexanes, the conductivity is enhanced, as shown in the Nyquist plots in

https://dx.doi.org/10.1021/acsomega.0c02794
ACS Omega 2020, 5, 20567–20574

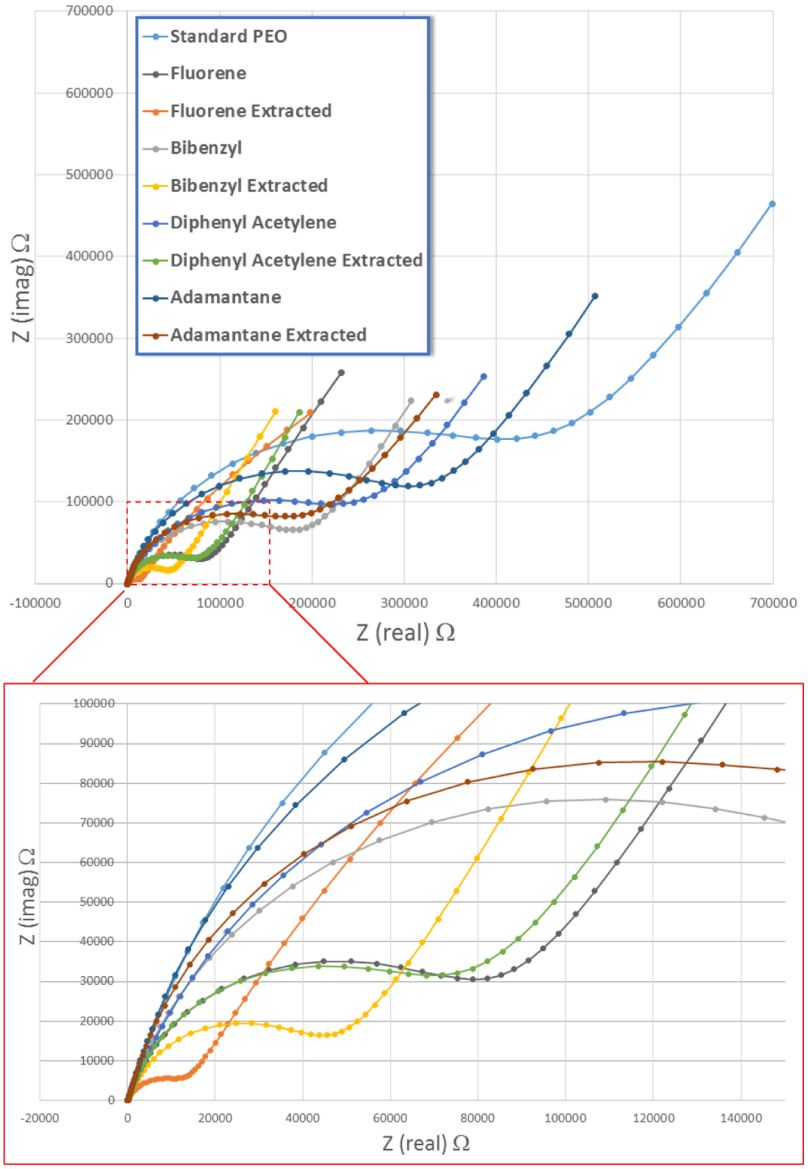

Figure 2. Nyquist plots of extracted and nonextracted films containing hydrocarbon nanofillers **1**−**4**.

Figure 2. Of hydrocarbons **1**−**4**, the nanofillers that result in the largest difference in conductivity between the extracted and nonextracted films are the examples that contain aromatic (phenyl) rings. The difference in conductivity also appears to be related to the percentage of the extracted hydrocarbon from the PEO−LiOTf film (Table 1; comparison of films **1b**, **2b**, **3b**, and **4b**). During the casting process in which the solvent is slowly evaporated and the mixture concentration steadily increases, the nanofiller hydrocarbons will either aggregate or dissolve into the PEO matrix in varying ratios. We speculate that the aromatic hydrocarbons (**1**−**3**) will aggregate and pack more readily because of stronger intermolecular interactions than the nonaromatic example, adamantane (**4**). A more thorough dispersal of the nanofiller hydrocarbon (as in adamantane) throughout the PEO bulk appears to lead to a decrease in extraction efficiency and thus an attenuated difference in conductivity between the extracted and nonextracted films (films **4a** and **4b**). The difference between extracted and nonextracted films is further summarized in Figure 3, in which the log of specific conductivity is plotted for hydrocarbons **1**−**4**.

Following these observations, a series of polar heteroarenes and heteroatom-containing aromatics were selected as hydro-

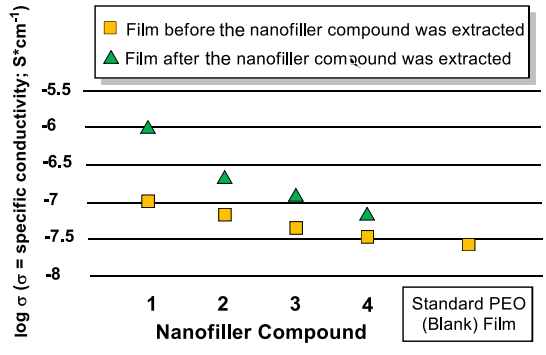

Figure 3. Summarized conductivity of extracted and nonextracted electrolyte films using hydrocarbons **1**−**4**.

https://dx.doi.org/10.1021/acsomega.0c02794
ACS Omega 2020, 5, 20567−20574

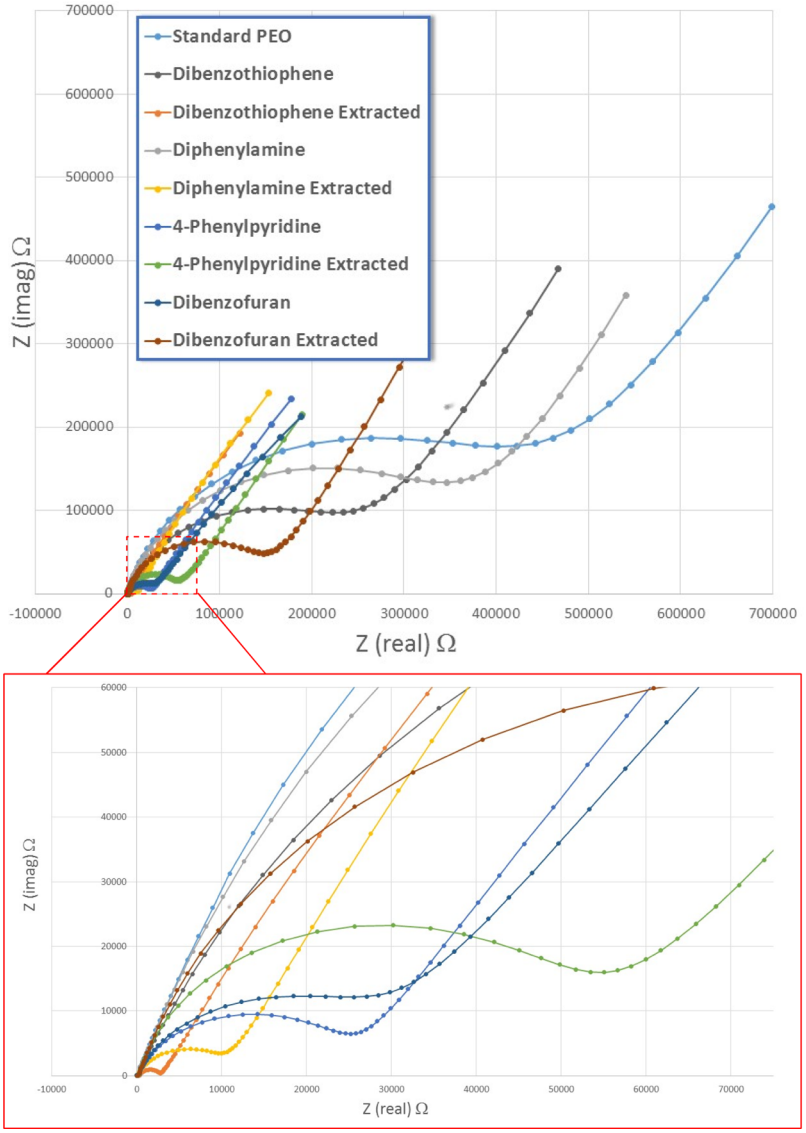

Figure 4. Nyquist plots of extracted and nonextracted films containing hydrocarbon nanofillers **5**−**8**.

carbon nanofillers. Dibenzofuran and dibenzothiophene (Figure 1; **5** and **8**) were selected as heteroarene analogues of fluorene that would potentially dissolve in the polar PEO matrix more readily and are capable of weakly coordinating a Li^+ ion. In addition, two nitrogen-containing aromatic hydrocarbons, 4-phenylpyridine and diphenylamine (Figure 1; **6** and **7**), were selected as strong Li^+ ion-coordinating examples for investigation. Films were prepared and extracted in a similar manner to the nonpolar hydrocarbons, and the results of the ac impedance investigation are shown in Figure 4.

The results of the conductivity studies are further summarized in Figure 5. Utilization of nanofiller compounds **5** and **6** provided evidence for a dramatic improvement of conductivity upon extraction of the nanofiller material from the film. The best results provide an increase over 2 orders of magnitude relative to the blank PEO−LiOTf film. Nanofiller compounds **7** and **8** effectively serve to increase conductivity relative to the standard (blank) PEO−LiOTf film when the nanofiller material was left in the film. Partial extraction of the nanofiller material resulted in an attenuation of the film conductivity, resulting in conductance values closer to that of the blank PEO−LiOTf film.

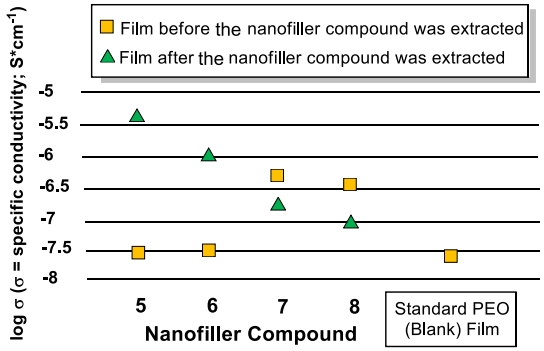

Figure 5. Summarized conductivity of extracted and nonextracted electrolyte films using hydrocarbons **5**−**8**.

The nanofiller extracted and nonextracted films were further analyzed using a variety of tools. Figure 6A shows a representative scanning electron microscopy (SEM) image of a film (**3a**) with clearly visible spherulites. In Figure 6B, the surface of a film (**1a**) with fluorene nanofiller aggregates visibly embedded on the film surface before extraction is shown. In

https://dx.doi.org/10.1021/acsomega.0c02794
ACS Omega 2020, 5, 20567−20574

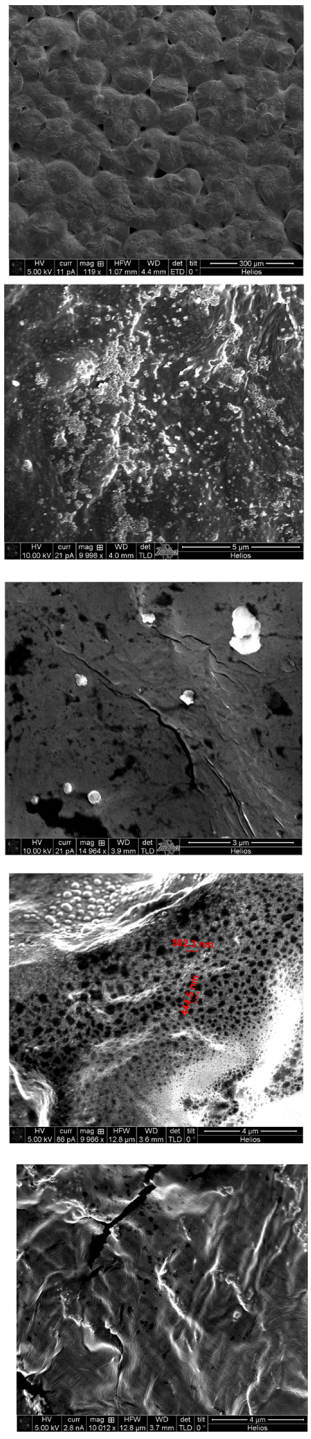

Figure 6. (A) SEM image (magnification 120×) of PEO−LiOTf film **3a** with the diphenylacetylene nanofiller (top surface) before extraction. (B) SEM image (magnification 10,000×) of PEO−LiOTf film **1a** with the fluorene nanofiller (bottom surface) before extraction. Surface aggregates are visible. (C) SEM image (magnification 5,000×) of PEO−LiOTf film **1b** with the fluorene nanofiller (bottom surface) after partial (85%) extraction. Surface aggregates and pits are visible. (D) SEM image (magnification 10,000×) of PEO−LiOTf film **2b** with the bibenzyl nanofiller (top surface) after partial (57%) extraction. Unremoved surface aggregates along with aggregate-sized cavities are visible after the extraction process. (E) SEM image (magnification 10,000×) of a cross section (break line perpendicular to the evaporation surface) of PEO−LiOTf film **2b** with the bibenzyl nanofiller after partial (57%) extraction. Aggregates and pits are visible in the interior of the film.

Figure 6C, the surface of a film (**1b**) where fluorene was embedded and then partially (85% by mass) extracted is shown. Identifiable pores on the surface following the extraction of the filler compound are observable, along with remaining fluorene aggregates for size comparison. An additional example of a partially extracted surface of a film is shown in Figure 6D. A PEO−LiOTf film (**2b**) with bibenzyl nanofiller partially (57% by mass) extracted displays unremoved aggregates along with aggregate-sized cavities that have resulted from the extraction process. In addition to an increase in surface porosity, pores and cavities in the interior of the bulk film have been observed in SEM images of a film edge (cross section) of extracted film **2b**, as shown in Figure 6E.

Additional SEM images can be found within the Supporting Information. Of particular note are the degrees to which the hydrocarbon additives aggregate on the surface. Adamantane, dibenzofuran, and fluorene appear on the film surface as a more finely dispersed "powdery" material, while 4-phenylpyridine, dibenzothiophene, bibenzyl, and diphenylacetylene appear as congregated islands of the aggregated material on the surface (Figures S5A−C, S6A−C, and S7A−D of the Supporting Information). The surface of a dibenzothiophene-embedded film appears to have the aggregate islands embedded further into the film surface compared to other films. This characteristic may potentially result in deeper pores and cavities upon extraction and thus the substantial increase in conductivity following extraction (Figure S8A−D of the Supporting Information).

Further characterizational studies were conducted using atomic force microscopy (AFM). As shown in Figure S9A,B of the Supporting Information, pores and cavities that result after hydrocarbon extraction are similar in size to the observed (by SEM) aggregates on the film surface. Last, the thermal properties of the films with nanofiller materials were determined by differential scanning calorimetry (DSC). Both the extracted and nonextracted films display similar crystallinity to the blank PEO−LiOTf film. This is shown by the fact that the spherulite morphologies of the nanofiller films (Figure S2A,C in the Supporting Information representative of all nanofiller films) are all similar to that of the blank film (Figure 6A) and that the PEO crystalline melting temperatures were virtually identical for the blank film and all films with nanofillers (Figure S19A−G in the Supporting Information). However, thermal data indicate some changes in the amorphous polymer behavior. The glass-transition temperatures, T_g, for all films studied exhibited a decrease with the filler or without the filler. In general, however, films that have the filler removed had larger reductions in the T_g. Because the films that had the fillers extracted also had the largest increase in conductivity; the glass-transition data for films (**1b**−**8b**) where the nanofiller had been removed are only shown in Figure 7. The T_g for a pure PEO electrolyte film is also shown for comparison. As can be seen, the T_g decreases for all the systems. The fact that the addition and then the removal of the nanofiller decrease the glass transition indicates enhanced segmental motion of the polymer backbone and should favor enhanced ionic conduction. Enhanced backbone motion would be considered a potential benefit of all these filler systems to ion conduction. However, the drop in the glass transition at its maximum value is only 6 °C, which is not sufficient to explain the increase observed in some of the systems.

The increase in ion conduction with the extraction of the nanofiller is an interesting phenomenon. One way of

https://dx.doi.org/10.1021/acsomega.0c02794
ACS Omega 2020, 5, 20567−20574

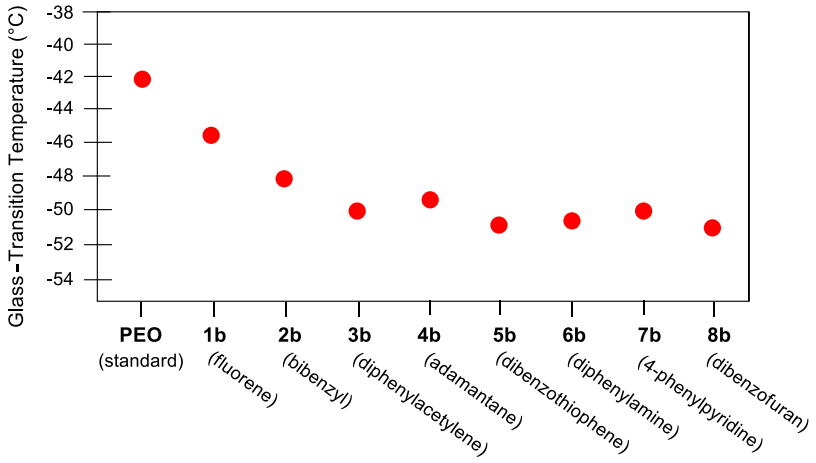

Figure 7. Comparison of glass-transition temperatures (T_g) from films **1b**−**8b** after extraction of the nanofiller.

interpreting this involves the considerations of the surfaces involved. The interfacial region between a polymer electrolyte surface and the surface of a second, high surface energy phase such as alumina has been attributed to interesting changes in ion conduction when compared to pure bulk polymer conduction values.[30−33,39−41] In this case, the strong interactions between the polymer and the high surface energy phase can cause regions of higher crystallinity and regions where the polymer backbone motions are hindered for a short distance into the PEO matrix. Both factors can reduce ion conduction in this region.[32] In the PEO electrolytes studied here, extraction of the nanofiller creates an interfacial region in the PEO caused by the interface between the solid PEO and the empty space of the removed filler. Inherently, the empty space would provide a surface of low surface energy. Perhaps this much different interface, the interface between the polymer electrolyte and the empty space, actually enhances ion conduction in these empty space systems. Previous research has shown that the concentration of free ions is increased relative to the concentrations of ion pairs and ion aggregates at such interfaces.[42] Because an increase in the concentration of free lithium ions in a polymer electrolyte is known to increase ion conduction,[43] this intensification in free lithium ion concentration at the interface could be one reason for the increased ion conduction in these systems. The concept of polymer electrolytes with these types of interfaces and a resulting increase in ion conduction warrants further research.

CONCLUSIONS

In conclusion, we report the use of innocuous nonpolar solvents for the intentional extraction of hydrocarbon nanofillers that have disrupted PEO constitution. An increase in surface and bulk porosity has been observed by SEM following partial extraction of an embedded hydrocarbon. By employing this strategy, we have observed a conductivity over 2 logarithmic orders of magnitude in extracted films. It is expected that this is an approach that will lead to further studies involving the operationally simple production of inexpensive electrolyte films with enhanced conductivity. Further investigations toward mixed/multinanofiller films, surface versus bulk conduction, and cavity formation will provide valuable information regarding surface/bulk porosity of polymeric films in a cost-effective method of preparation.

EXPERIMENTAL SECTION

Materials and Instrumentation. All reagents and solvents were purchased from commercial sources and used without further purification. PEO, with a typical molecular weight of 1 M, was purchased from Sigma-Aldrich. Poly(tetrafluoroethylene) (PTFE) flat-form evaporating dishes were purchased from VWR and have the following dimensions: a capacity of 50 mL, a diameter of 60 mm, and a height of 20 mm. An image of the evaporating chamber is provided in the Supporting Information. Verification of the extracted nanofiller was conducted using ^{1}H NMR on a Varian 400/100 (400 MHz) spectrometer in deuterated chloroform ($CDCl_3$) with spectral comparison to the pure compound. Infrared spectra were recorded on a Nicolet iS50 Fourier-transform infrared spectrometer using an attenuated total reflection attachment, and the peaks are reported in reciprocal centimeters (cm^{-1}). A Solartron 1260 gain-phase analyzer with a 1296 dielectric interface was used for impedance spectroscopy measurements. TA Discovery Series 25 DSC and a TA model 5500 TGA were used to collect thermal analysis data.

General Preparation of Films. Polymer electrolyte films were prepared using a casting method in which PEO (0.330 g), LiOTf (0.0825 g, 0.529 mmol), and a nanofiller compound (0.106 mmol, 20 mol % relative to LiOTf) were homogeneously dissolved in 33 mL of optima grade acetonitrile under argon. The solution was stirred for 30 min to ensure that no globules of PEO remain and then poured into a PTFE evaporating dish (note—the PEO globules can be largely avoided by a very slow addition of PEO to acetonitrile while stirring). After evaporating acetonitrile under a flow of nitrogen for 48 h, films between 90 and 110 μm thickness were produced. The films were then submerged in and surrounded by 15−30 mL of hexanes warmed to 40 °C for 5−10 min and rinsed twice with room-temperature hexanes to extract nanofiller materials. The hexanes from the extracted solution were then evaporated under vacuum. The identity of the removed nanofiller was confirmed by ^{1}H NMR, and the quantity of the extract was determined by weighing the dried residual material. The leaching of LiOTf or PEO was not observed by ^{1}H NMR in any of the examples. The conductivity of the extracted and nonextracted PEO−LiOTf bulk films was measured using ac impedance. Each of the films with nanofiller materials was prepared in duplicate, and the ac impedance of the nonextracted and extracted films was measured separately.

https://dx.doi.org/10.1021/acsomega.0c02794
ACS Omega 2020, 5, 20567−20574

Edges for SEM cross-sectional images of PEO electrolytes were obtained by freezing the film in liquid nitrogen and breaking the film along a straight edge.

■ ASSOCIATED CONTENT

Supporting Information

The Supporting Information is available free of charge at https://pubs.acs.org/doi/10.1021/acsomega.0c02794.

Additional SEM images, AFM images, DSC plots, GA, and expanded Nyquist plots (PDF)

■ AUTHOR INFORMATION

Corresponding Authors

Dale Teeters − *Department of Chemistry and Biochemistry, The University of Tulsa, Tulsa, Oklahoma 74104, United States*; Email: dale-teeters@utulsa.edu

Angus A. Lamar − *Department of Chemistry and Biochemistry, The University of Tulsa, Tulsa, Oklahoma 74104, United States*; orcid.org/0000-0002-2962-0137; Email: angus-lamar@utulsa.edu

Authors

John W. Ostrander − *Department of Chemistry and Biochemistry, The University of Tulsa, Tulsa, Oklahoma 74104, United States*

Lei Wang − *Department of Chemistry and Biochemistry, The University of Tulsa, Tulsa, Oklahoma 74104, United States*

Teljan Ali Kizi − *Department of Chemistry and Biochemistry, The University of Tulsa, Tulsa, Oklahoma 74104, United States*

Jana A. Dajani − *Department of Chemistry, Hanover College, Hanover, Indiana 47243, United States*

Austin V. Carr − *Department of Chemistry and Biochemistry, The University of Tulsa, Tulsa, Oklahoma 74104, United States*

Complete contact information is available at: https://pubs.acs.org/10.1021/acsomega.0c02794

Notes

The authors declare no competing financial interest.

■ ACKNOWLEDGMENTS

The authors would like to acknowledge members of the University of Tulsa Nanotechnology Institute for support and useful discussion from its members. J.W.O. would like to thank the University of Tulsa Graduate School and the Office of Research for travel funding for promoting this work. This work was supported in part by the Oklahoma Center for the Advancement of Science and Technology (OCAST) and NASA grant no. NNX13AN01A issued through the NASA EPSCoR Program. A.A.L. is grateful for the financial support provided by the lab start-up contribution from the University of Tulsa. In addition, J.A.D. would like to acknowledge the Hanover College Richter Grant award for support. Finally, the authors would also like to thank the University of Tulsa Chemistry Summer Undergraduate Research Program (CSURP) for support.

■ REFERENCES

(1) Tarascon, J.-M.; Armand, M. Issues and challenges facing rechargeable lithium batteries. *Nature* **2001**, *414*, 359.

(2) Scrosati, B. Power sources for portable electronics and hybrid cars: lithium batteries and fuel cells. *Chem. Rec.* **2005**, *5*, 286−297.

(3) Dunn, B.; Kamath, H.; Tarascon, J.-M. Electrical Energy Storage for the Grid: A Battery of Choices. *Science* **2011**, *334*, 928−935.

(4) Meyer, W. H. Polymer Electrolytes for Lithium-Ion Batteries. *Adv. Mater.* **1998**, *10*, 439−448.

(5) Dias, F. B.; Plomp, L.; Veldhuis, J. B. J. Trends in polymer electrolytes for secondary lithium batteries. *J. Power Sources* **2000**, *88*, 169−191.

(6) Armand, M.; Tarascon, J.-M. Building better batteries. *Nature* **2008**, *451*, 652.

(7) Cheng, X.-B.; Zhang, R.; Zhao, C.-Z.; Zhang, Q. Toward Safe Lithium Metal Anode in Rechargeable Batteries: A Review. *Chem. Rev.* **2017**, *117*, 10403−10473.

(8) Angell, C. A.; Liu, C.; Sanchez, E. Rubbery solid electrolytes with dominant cationic transport and high ambient conductivity. *Nature* **1993**, *362*, 137.

(9) For recent reviews, see: (a) Jiang, Y.; Yan, X.; Ma, Z.; Mei, P.; Xiao, W.; You, Q.; Zhang, Y. Development of the PEO Based Solid Polymer Electrolytes for All-Solid State Lithium Ion Batteries. *Polymers* **2018**, *10*, 1237. (b) Wan, J.; Xie, J.; Mackanic, D. G.; Burke, W.; Bao, Z.; Cui, Y. Status, promises, and challenges of nanocomposite solid-state electrolytes for safe and high performance lithium batteries. *Mater. Today Nano* **2018**, *4*, 1−16. (c) Austen Angell, C. Concepts and conflicts in polymer electrolytes: The search for ion mobility. *Electrochim. Acta* **2019**, *313*, 205−210. (d) Zhou, Q.; Ma, J.; Dong, S.; Li, X.; Cui, G. Intermolecular Chemistry in Solid Polymer Electrolytes for High-Energy-Density Lithium Batteries. *Adv. Mater.* **2019**, *31*, 1902029.

(10) Shin, D. W.; Guiver, M. D.; Lee, Y. M. Hydrocarbon-Based Polymer Electrolyte Membranes: Importance of Morphology on Ion Transport and Membrane Stability. *Chem. Rev.* **2017**, *117*, 4759−4805.

(11) Kim, S.-K.; Kim, D.-G.; Lee, A.; Sohn, H.-S.; Wie, J. J.; Nguyen, N. A.; Mackay, M. E.; Lee, J.-C. Organic/Inorganic Hybrid Block Copolymer Electrolytes with Nanoscale Ion-Conducting Channels for Lithium Ion Batteries. *Macromolecules* **2012**, *45*, 9347−9356.

(12) Sheldon, M.; Glasse, M.; Latham, R.; Linford, R. The effect of plasticiser on zinc polymer electrolytes. *Solid State Ionics* **1989**, *34*, 135−138.

(13) Yang, X. Q.; Lee, H. S.; Hanson, L.; McBreen, J.; Okamoto, Y. Development of a new plasticizer for poly(ethylene oxide)-based polymer electrolyte and the investigation of their ion-pair dissociation effect. *J. Power Sources* **1995**, *54*, 198−204.

(14) Croce, F.; Appetecchi, G. B.; Persi, L.; Scrosati, B. Nanocomposite polymer electrolytes for lithium batteries. *Nature* **1998**, *394*, 456.

(15) Manuel Stephan, A.; Nahm, K. S. Review on composite polymer electrolytes for lithium batteries. *Polymer* **2006**, *47*, 5952−5964.

(16) Ahn, J.-H.; Wang, G. X.; Liu, H. K.; Dou, S. X. Nanoparticle-dispersed PEO polymer electrolytes for Li batteries. *J. Power Sources* **2003**, *119*−*121*, 422−426.

(17) Weston, J.; Steele, B. Effects of inert fillers on the mechanical and electrochemical properties of lithium salt-poly(ethylene oxide) polymer electrolytes. *Solid State Ionics* **1982**, *7*, 75−79.

(18) Chen, H.-W.; Chiu, C.-Y.; Wu, H.-D.; Shen, I.-W.; Chang, F.-C. Solid-state electrolyte nanocomposites based on poly(ethylene oxide), poly(oxypropylene) diamine, mineral clay and lithium perchlorate. *Polymer* **2002**, *43*, 5011−5016.

(19) Sandí, G.; Carrado, K. A.; Joachin, H.; Lu, W.; Prakash, J. Polymer nanocomposites for lithium battery applications. *J. Power Sources* **2003**, *119*−*121*, 492−496.

(20) Panday, A.; Mullin, S.; Gomez, E. D.; Wanakule, N.; Chen, V. L.; Hexemer, A.; Pople, J.; Balsara, N. P. Effect of Molecular Weight and Salt Concentration on Conductivity of Block Copolymer Electrolytes. *Macromolecules* **2009**, *42*, 4632−4637.

(21) Singh, M.; Odusanya, O.; Wilmes, G. M.; Eitouni, H. B.; Gomez, E. D.; Patel, A. J.; Chen, V. L.; Park, M. J.; Fragouli, P.;

Iatrou, H.; Hadjichristidis, N.; Cookson, D.; Balsara, N. P. Effect of Molecular Weight on the Mechanical and Electrical Properties of Block Copolymer Electrolytes. *Macromolecules* **2007**, *40*, 4578−4585.
(22) Choi, I.; Ahn, H.; Park, M. J. Enhanced Performance in Lithium-Polymer Batteries Using Surface-Functionalized Si Nanoparticle Anodes and Self-Assembled Block Copolymer Electrolytes. *Macromolecules* **2011**, *44*, 7327−7334.
(23) Gomez, E. D.; Panday, A.; Feng, E. H.; Chen, V.; Stone, G. M.; Minor, A. M.; Kisielowski, C.; Downing, K. H.; Borodin, O.; Smith, G. D.; Balsara, N. P. Effect of Ion Distribution on Conductivity of Block Copolymer Electrolytes. *Nano Lett.* **2009**, *9*, 1212−1216.
(24) Kim, H.-C.; Park, S.-M.; Hinsberg, W. D. Block Copolymer Based Nanostructures: Materials, Processes, and Applications to Electronics. *Chem. Rev.* **2010**, *110*, 146−177.
(25) Hou, X.; Siow, K. S. Ionic conductivity and electrochemical characterization of novel interpenetrating polymer network electrolytes. *Solid State Ionics* **2002**, *147*, 391−395.
(26) Oh, B.; Vissers, D.; Zhang, Z.; West, R.; Tsukamoto, H.; Amine, K. New interpenetrating network type poly(siloxane-g-ethylene oxide) polymer electrolyte for lithium battery. *J. Power Sources* **2003**, *119*−*121*, 442−447.
(27) Capuano, F.; Croce, F.; Scrosati, B. Composite Polymer Electrolytes. *J. Electrochem. Soc.* **1991**, *138*, 1918−1922.
(28) Tominaga, Y.; Asai, S.; Sumita, M.; Panero, S.; Scrosati, B. A novel composite polymer electrolyte: Effect of mesoporous SiO_2 on ionic conduction in poly(ethylene oxide)−$LiCF_3SO_3$ complex. *J. Power Sources* **2005**, *146*, 402−406.
(29) Jeon, J.-D.; Kwak, S.-Y.; Cho, B.-W. Solvent-Free Polymer Electrolytes: I. Preparation and Characterization of Polymer Electrolytes Having Pores Filled with Viscous P(EO - EC)/ $LiCF_3SO_3$. *J. Electrochem. Soc.* **2005**, *152*, A1583−A1589.
(30) Vorrey, S.; Teeters, D. Study of the ion conduction of polymer electrolytes confined in micro and nanopores. *Electrochim. Acta* **2003**, *48*, 2137−2141.
(31) Bishop, C.; Teeters, D. Crystallinity and order of poly(ethylene oxide)/lithium triflate complex confined in nanoporous membranes. *Electrochim. Acta* **2009**, *54*, 4084−4088.
(32) Abudakka, M.; Decker, D. S.; Sutherlin, L. T.; Teeters, D. Ceramic/polymer interpenetrating networks exhibiting increased ionic conductivity with temperature control of ion conduction for thermal runaway protection. *Int. J. Hydrogen Energy* **2014**, *39*, 2988−2996.
(33) Jayasekara, I.; Poyner, M.; Teeters, D. Investigation of a nanoconfined, ceramic composite, solid polymer electrolyte. *Electrochim. Acta* **2017**, *247*, 1147−1154.
(34) Trifkovic, M.; Hedegaard, A.; Huston, K.; Sheikhzadeh, M.; Macosko, C. W. Porous Films via PE/PEO Cocontinuous Blends. *Macromolecules* **2012**, *45*, 6036−6044.
(35) Ortel, E.; Reier, T.; Strasser, P.; Kraehnert, R. Mesoporous IrO_2 Films Templated by PEO-PB-PEO Block-Copolymers: Self-Assembly, Crystallization Behavior, and Electrocatalytic Performance. *Chem. Mater.* **2011**, *23*, 3201−3209.
(36) Choukourov, A.; Gordeev, I.; Ponti, J.; Uboldi, C.; Melnichuk, I.; Vaidulych, M.; Kousal, J.; Nikitin, D.; Hanyková, L.; Krakovský, I.; Slavínská, D.; Biederman, H. Microphase-Separated PE/PEO Thin Films Prepared by Plasma-Assisted Vapor Phase Deposition. *ACS Appl. Mater. Interfaces* **2016**, *8*, 8201−8212.
(37) Wu, D.; Xu, F.; Sun, B.; Fu, R.; He, H.; Matyjaszewski, K. Design and preparation of porous polymers. *Chem. Rev.* **2012**, *112*, 3959−4015.
(38) Yoshikawa, M.; Tharpa, K.; Dima, Ş.-O. Molecularly Imprinted Membranes: Past, Present, and Future. *Chem. Rev.* **2016**, *116*, 11500−11528.
(39) Kasemägi, H.; Klintenberg, M.; Aabloo, A.; Thomas, J. O. Molecular dynamics simulation of the $LiBF_4$−PEO system containing Al_2O_3 nanoparticles. *Solid State Ionics* **2002**, *147*, 367−375.
(40) Kasemägi, H.; Aabloo, A.; Klintenberg, M. K.; Thomas, J. O. Molecular dynamics simulation of the effect of nanoparticle fillers on ion motion in a polymer host. *Solid State Ionics* **2004**, *168*, 249−254.
(41) van Eijck, L.; Best, A. S.; Stride, J.; Kearley, G. J. Softening of the potential-energy surface in polymer electrolytes on the addition of nanoparticles. *Chem. Phys.* **2005**, *317*, 282−288.
(42) Teeters, D.; Neuman, R. G.; Tate, B. D. The Concentration Behavior of Lithium Triflate at the Surface of Polymer Electrolyte Materials. *Solid State Ionics* **1996**, *85*, 239.
(43) MacCallum, J. R.; Vincent, C. A. *Polymer Electrolyte Reviews*; MacCallum, J. R., Vincent, C. A., Eds.; Elsevier: London and New York, 1987; Vol. *1*, p 23.

https://dx.doi.org/10.1021/acsomega.0c02794
ACS Omega 2020, 5, 20567−20574